Science of the Total Environment 833 (2022) 155224

Contents lists available at ScienceDirect

Science of the Total Environment

journal homepage: www.elsevier.com/locate/scitotenv

Stream-pit lake interactions in an abandoned mining area affected by acid drainage (Iberian Pyrite Belt)

Jose M. Fuentes-López, Manuel Olías, Rafael León, Maria Dolores Basallote, Francisco Macías, Raul Moreno-González, Carlos R. Cánovas *

Department of Earth Sciences & Research Center on Natural Resources, Health and the Environment, University of Huelva, Campus 'El Carmen', 21071, Huelva, Spain

HIGHLIGHTS

- Hydrological connections between surface and groundwater in a pit lake were studied.
- Geochemical tracers identified the predominance of surface waters in the system.
- High contaminant loads released from the mining area (e.g., 520 kg/day of Fe).
- Geochemical tracers allowed identifying pollutant sources in the system.
- Most of released pollutants come from waste dumps in the vicinity of the pit lake.

GRAPHICAL ABSTRACT

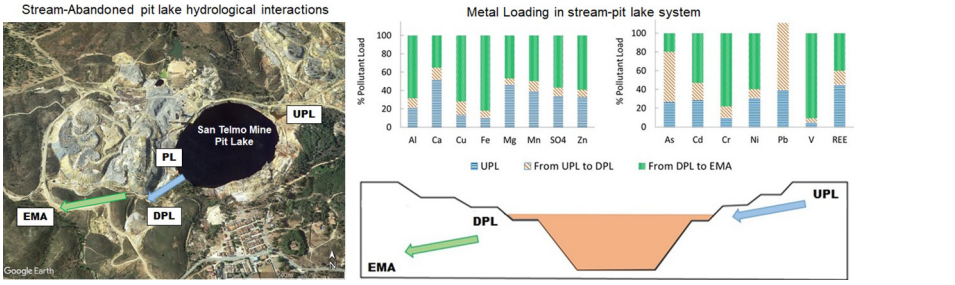

ARTICLE INFO

Editor: José Virgílio Cruz

Keywords:
Sulfide opencast mining
Water pollution
Trace elements
Rare earth elements
Acidic pit lake

ABSTRACT

Opencast mining of sulfide ore deposits may lead to the formation of anthropogenic acidic lakes with highly polluted waters. In these systems, it is crucial to understand the hydrological connections between surface and groundwater and their contribution to the pollutant load delivered to the downgradient streams. This study characterizes the interactions between surface and groundwater in an acidic pit lake using different geochemical tracers (i.e., REE and other trace metals). The San Telmo pit lake, located in one of the most pollutant sources of the Iberian Pyrite Belt (IPB), can be considered as a flow-through pit lake except during dry periods, when it behaves as a terminal lake due to lower inputs by surface waters and higher outputs by evaporation. Results based on geochemical tracers indicate that the main inputs to the pit lake come from surface waters, with minor groundwater inputs rich in As, Cr, Cu, Fe and Pb. The contaminant load released from the mining area is very high (e.g., median values of 520 kg/day of Fe and 38 kg/day of Zn), causing the degradation of the fluvial network downstream. Most of released pollutants come from waste dumps located at the W of the mining zone (~50–70% of Al, Cd, Mg, Mn, Ni, SO_4 and Zn and > 70% for Cu, Cr, Fe and, V), while the contribution of the water coming out the pit lake and other dumps is much lower. Thus, remediation efforts to improve the area and fluvial courses downstream must focus on the W waste dumps.

1. Introduction

Intense mining of sulfide deposits worldwide, especially since the second half of the 19th century, has left a legacy of abandoned mines with huge sulfide-bearing waste rock piles exposed to weathering agents and open pits. The cessation of mining activities in open pits often leads to the recovery of the original water table and their flooding, creating pit lakes (McCullough, 2015; Triantafyllidis and Skarpelis, 2006). The presence of acidifying minerals, especially in sulfide and coal mining, may lead to the acidification of pit lake waters (pH < 4) and the existence of high concentrations of dissolved metal(*oid*)s, degrading these water resources worldwide (e.g. Pellicori et al., 2005; Sánchez España et al., 2005 and 2008; Ríos et al., 2008; Zhao et al., 2012; Tomiyama et al., 2019; Luo et al., 2020; Rinder et al., 2020).

* Corresponding author.
E-mail address: carlos.ruiz@dgeo.uhu.es (C.R. Cánovas).

http://dx.doi.org/10.1016/j.scitotenv.2022.155224
Received 24 January 2022; Received in revised form 18 March 2022; Accepted 8 April 2022
Available online 12 April 2022

Water quality of a pit lake strongly depends on the balance between acidity and alkalinity inputs, as well as the neutralization processes that may take place within the water column (Castendyk et al., 2015; Schafer et al., 2020). Regarding acidifying reactions, the oxidation of pyrite (FeS_2) by oxygen plays a key role in acid mine drainage (AMD) generation (Johnson and Hallberg, 2005):

$$FeS_{2(s)} + 15/4\ O_{2(g)} + 7/2\ H_2O_{(l)} \rightarrow Fe(OH)_{3(s)} + 2SO^{2-}_{4(aq)} + 4H^{+}_{(aq)} \quad (1)$$

In addition, a limited oxygen renewal in underground environments (such as lower layers of a pit lake) can decrease considerably the concentration of oxygen in the acidic waters, acting Fe^{3+} as predominant oxidant agent of pyrite (reaction 2). This reaction is notwithstanding limited by the oxidation of Fe^{2+} to Fe^{3+}, which can be enhanced by the activity of extremophile microorganisms such as Acidithiobacilus *thiooxidans* or Chlamydomonas *acidophila*, acting as a reaction catalysts under low pH range (<4) in aerobic environments (Wendt-Potthoff et al., 2012; Valente et al., 2013).

$$FeS_{2(s)} + 14Fe^{3+}_{(aq)} + 8H_2O_{(l)} \rightarrow 15Fe^{2+}_{(aq)} + 2SO^{2-}_{4(aq)} + 16H^{+}_{(aq)} \quad (2)$$

The precipitation of secondary Fe minerals in the water column may provide additional acidity to the waters, exerting in many cases a buffer pH in sulfide pit lakes (Sánchez España et al., 2008 and 2011; Elghali et al., 2021; Fan et al., 2022). The generated leachates may attack the host rock of the ore deposits, dissolving also Al, Mg, Mn, Si and other elements into the pit lake waters. The dissolution of the host rock minerals usually consumes acidity, but its different dissolution kinetic compared to sulfide oxidation makes the overall reactions distinctly acidic. Other reactions may also generate alkalinity to counteract the acidity released during sulfide oxidation such as sulfate reduction or cation-exchange reactions (Blodau, 2006; Torres et al., 2013).

Despite the huge volume of acidic waters stored and the high number of pit lakes found worldwide, the hydrological connections between surface and groundwater and their relative contributions to pit lakes and downgradient stream systems are site specific and not completely understood (Newman et al., 2020). This information is of paramount importance to adopt effective remediation measures in abandoned mine sites worldwide. In this sense, geochemical tracers have been shown as useful tools to establish hydrological connections in aquatic systems (e.g., Erostate et al., 2019; Yang et al., 2021) especially in AMD environments (Cánovas et al., 2016; Moreno González et al., 2020a, 2020b).

The Iberian Pyrite Belt (IPB, SW Spain) is one of the largest polymetallic massive sulfide-mining provinces in the world (Almodóvar et al., 2019), which has been intensively exploited since ancient times. As a result, a legacy of derelict mines with large accumulation of sulfide mining wastes has caused a severe deterioration of the main fluvial systems in the region, i.e., the Tinto and Odiel rivers (Sánchez España et al., 2005; Sarmiento et al., 2009; Moreno González et al., 2018; Olías et al., 2019 and Olías et al., 2020). There are 22 different flooded open pits only in the Spanish part of the IPB (Sánchez España et al., 2008), which makes it a representative worldwide example to study hydrological connections between surface and groundwater in pit lakes. Among them, San Telmo pit lake is the largest accumulation of acidic water (Diez Ercilla et al., 2009; Sánchez España et al., 2007, 2008 and Sánchez-España et al., 2011; Cánovas et al., 2015). Therefore, the goal of the present study is to analyze by using geochemical tracers the interactions of surface waters - pit lake in San Telmo mine and, specifically, the contribution of the pit lake in the contaminant load generated in the whole area.

2. Site description

The IPB extends from the western side of the Seville province to the Atlantic ocean in the Portuguese coast, approximately 250 km long and 25 to 70 km wide (Donaire et al., 2020). It includes three different lithological units: (1) the Phyllitic-Quartzitic Group formed by a thick sequence of Devonian phyllites and quartzites; (2) the Volcano-Sedimentary Complex (VSC) composed of shales, greywackes and alternate layers of Upper Devonian-Lower Carboniferous felsic (mainly dacites and rhyolites) and mafic rocks (mainly basaltic sills); and finally (3) the Culm Group at the very top of the column with Carboniferous detrital sediments (shales and conglomerates) (Almodóvar et al., 2019). The massive sulfide deposits are associated to the CVS and composed mainly of fine grained pyrite (FeS_2) (approximately >90% in volume), with lower amounts of sphalerite (ZnS), chalcopyrite ($CuFeS_2$) and galena (PbS). It is worth to notice the abundance of aluminosilicates as gangue minerals, as well as the low concentration of carbonates, allowing extreme acidic conditions (Sánchez España et al., 2008; Moreno González et al., 2020a).

Regarding the climate, due to Mediterranean conditions, the average temperature is around 17 °C while the average rainfall is close to 740 mm, with high inter and intra-annual variability (Galván et al., 2016). Winters are relatively cold (with average minimum temperatures close to 6 °C) and humid, while summers are hot (average maximum temperatures close to 33 °C) with long drought periods.

There was evidence of early exploitation in San Telmo mine approximately 3000 years ago, which was followed by Romans (Pinedo Vara, 1963). However, it was in 1859 when the more intense period of mining began, especially from 1970's, with the excavation of a large open pit, to the end of mining in 1989. Then, the flooding of the open pit began. From an available ortophotograph in 1998 it can be seen that the pit lake was already completely formed (Fig. SM1), maintaining its dimensions to nowadays (approximately 500 m long and 370 m wide; Fig. 1), with a total surface of 0.18 km^2. According to Diez Ercilla et al. (2009), the flooding was mainly due to groundwater inputs. The maximum pit lake water depth is around 130 m (Cánovas et al., 2015), constituting the largest accumulation of acidic water in the IPB (8×10^6 m^3). The pit lake has been classified as meromictic, with a boundary layer at a depth of 29 m which separates and upper, oxygenated, lower density mixolimnion from an anoxic and higher density monimolimnion (Diez Ercilla et al., 2009; Sánchez España et al., 2007, 2008, 2009 and Sánchez-España et al., 2011; Cánovas et al., 2015).

There are two large waste dump areas, located to the northeast and to the west of the pit lake (Fig. 1), with a total surface of 0.76 km^2. Acidic discharges from the northeast dumps enters the pit lake through its east side (Fig. SM2). At its western side, there is a water output forming a small creek, which downstream also collects acidic waters from the western dumps (Fig. 1). Thus, the pit lake is defined as a flow-through type (Castendyk et al., 2015). The acidic waters released from San Telmo constitute one of the main pollutant sources in the area, causing the total degradation of the Oraque River, a tributary of the Odiel River (Sánchez España et al., 2005; Sarmiento et al., 2009; Galván et al., 2016). This tributary will feed a reservoir which is currently under construction, and there are serious doubts about the final quality of the stored waters (Olías et al., 2011).

3. Materials and methods

3.1. Samplings

The main AMD sources in San Telmo mine were studied during two years (from February 2018 to February 2020). A synoptic sampling was performed in four different sampling points (Fig. 1 and Fig. SM2): 1) Upstream Pit Lake (UPL), located in the NE area of San Telmo mine, where several small AMD flows emerge from mine dumps, entering the pit lake; 2) Pit Lake sampling point (PL), taken directly from the lake surface (epilimnion) just in the overflow zone (W of the pit lake); 3) Downstream Pit Lake (DPL), located approximately 250 m west from the pit lake; and finally, 4) the End of Mining Area (EMA) sampling point, located at the outlet of the mining zone, collecting all the acidic waters generated in the area. The sampling was performed twice per month during wet periods and monthly in the dry periods. The number of collected samples varied between 20 and 33 samples, as some sampling points were dried up during the dry season.

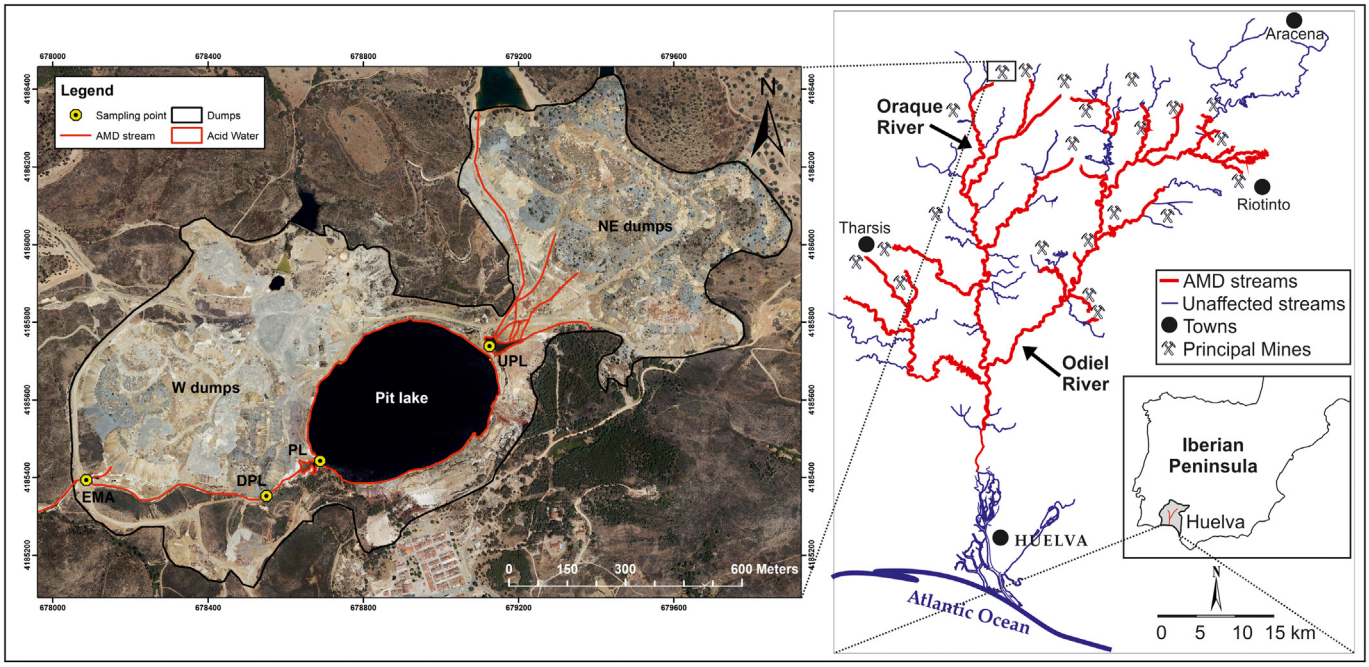

Fig. 1. Aerial photo of San Telmo mine in 2016, indicating the pit lake, dumps and the sampling points.

The precipitation values were collected from a weather station located at 14 km from the study area and flow rate (Q) was obtained by means of current meters (Global Water model FP111 and electromagnetic induction model OTT MF pro) and the estimation of the channel section. Different physico-chemical parameters (pH, electrical conductivity –EC-, oxidation-reduction potential –ORP- and temperature) were measured in situ with a CrisonMM40+ multimeter, previously calibrated with certified solutions. Eh values were obtained from the ORP values measured in the field according to Nordstrom and Wilde (1998). Samples were filtered through 0.45 μm filters, acidified to pH < 2 and conserved at 4 °C in high-density polyethylene bottles, previously washed with a solution of 10% HNO_3.

3.2. Laboratory analysis and data treatment

Sample analysis were performed at the R + D laboratories at the University of Huelva by: (1) Inductively Coupled Plasma-Atomic Emission Spectroscopy (ICP-OES) for Al, Ca, Cu, Fe, K, Na, Mg, Mn, S, Si and Zn; and (2) Inductively Coupled Plasma-Mass Spectroscopy (ICP-MS) for As, Cd, Cr, Li, Ni, Pb, Se, Sr, V, REE and U. The sulfate concentration was determined by the stoichiometric relationship (1:3) between sulfate and sulfur in samples due to the strongly oxidant conditions existent. Detection limits were 0.2 mg/L for Al, Ca, Fe, K, Mg, Mn, Na, Si and S; 50 μg/L for Zn; 5 μg/L for Cu, 1 μg/L for Se, Sr, La, Ce, Nd, Pr and Sm, and 0.2 μg/L for As, Cd, Cr, Ni, Pb V, Eu, Gd, Tb, Dy, Ho, Er, Tm, Yb and Lu. However, these limits may increase due to the dilution factor applied to certain highly metal-rich samples during the analysis. NIST-1640 certificate was used to verify the quality of analysis, with measures within ±5 of certified values. Analysis were performed in triplicate to evaluate analytical precision, which was better than 5% in every case. For each analysis sequence, homemade standards (from certified materials) and blanks were used to check the accuracy, and all elements were below the detection limit of the equipment.

The PHREEQC code v2.12.01 (Parkhurst and Appelo, 2013) was used to obtain the chemical speciation and saturation indices of waters. The Wateq4f database was enlarged with thermodynamic data from Yu et al. (1999) for the solubility of schwertmannite. For the assessment of metal transport during each sampling, the pollutant load was calculated by multiplying the flow rate by the concentration of each element. The net acidity (NA) of samples was determined by using the equation from Kirby and Cravotta (2005) (metal concentrations in mg/L):

$$NA(\text{as mg/L of } CaCO_3) = 50\left\{1000 \cdot \left(10^{-pH}\right) + \left[2\left(Fe^{II}\right) + 3\left(Fe^{III}\right)\right]/56 + 2(Mn)/55 + 3(Al)/27\right\}$$

REE normalized concentrations were obtained by using the North American Shale Composite (NASC) values from Taylor and McLennan (1985). Cerium (Ce) and Europium (Eu) anomalies were calculated by the following equations: $Ce_N/\sqrt{[La_N \cdot Pr_N]}$ and $Eu_N/\sqrt{[Sm_N \cdot Gd_N]}$ respectively, where the subscript N indicates normalized values.

4. Results and discussion

4.1. Rainfall evolution

Rainfall distribution during the study period was characterized by an irregular pattern (Fig. 2). February 2018 was dry, but at the beginning of March a rainy period began, which continued until the end of April (433 mm registered). The hydrological year 2018/19 was very dry (463

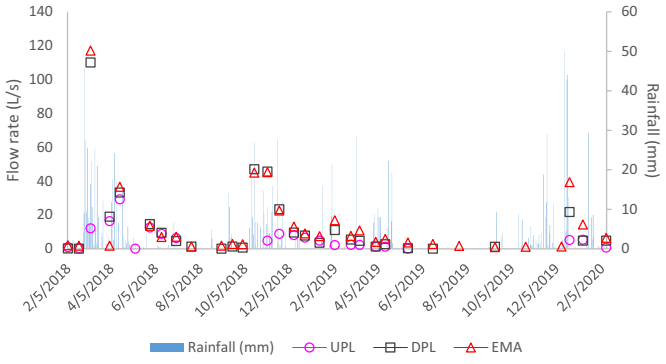

Fig. 2. Daily rainfall evolution and flow rate at the different sampling points during the study period.

mm), where most rainfalls occurred from October 2018 to April 2019. Finally, rainfall during hydrological year 2019/20 (640 mm) was also below the average value of the study area (740 mm), with most rainfall being recorded between autumn and winter (Fig. 2). The chemical composition of rainfall in the study area is characterized by circumneutral pH values (6.0–6.5) and low concentration of sulphate (<10 mg/L) and metals.

4.2. Physico-chemical parameters and dissolved concentrations

A clear relation between flow rate and rainfall distribution along the study period can be seen in Fig. 2. The UPL sampling point recorded the lowest flow rate values (median value of 2.3 L/s), while the flow rate increased downstream of the pit lake (median values of 4.8 L/s at DPL and 6.7 L/s at EMA). Water inputs into the pit lake through UPL were not permanent, as they ceased during summer. At the same time, water output by runoff from the pit lake ceased, thus making San Telmo pit lake to behave as a terminal lake due to a lack of surface water inputs and an increase of outputs by the intense evaporation.

In all the sampling points, pH values were very low (median between 2.3 and 2.8) and quite constant along the monitoring period (Table 1). A progressive decrease in pH values was observed downstream, showing the highest values in the pit lake entrance point (UPL, between 2.20 and 3.47) and the lowest at the end of the mining area (EMA, between 1.85 and 2.79). This increase in the acidic nature of AMD lixiviates was even more evident in the spatial evolution of net acidity, which varied from a median of 1.1 g/L of $CaCO_3$ at UPL to 4.8 g/L at EMA (Table 1).

The EC values showed the same tendency as the net acidity, experiencing an increase downstream of the pit lake. Thus, the lowest values were observed in UPL (median of 4.5 mS/cm) and the highest in EMA (8.8 mS/cm). Regarding Eh values, the highest oxidant conditions were observed at the pit lake (median of 773 mV), while the lowest were found in UPL and EMA (median values between 640 and 650 mV, Table 1). These higher Eh values in the pit lake waters may be related to the higher residence time of stored waters, which allows a more efficient oxygen renewal and Fe(II) oxidation than in running waters.

In regard of the temporal evolution, EC values showed relevant fluctuations in EMA (Fig. 3), experiencing an increase during dry periods (close to 12 mS/cm) and a decrease linked to dilution by high flows (especially during March–April and November–December 2018; Fig. 3). This tendency, although less pronounced, can be also observed in other sampling points. In this sense, the lower EC variations occurred in PL waters due to the buffering effect exerted by the high water volume stored in the epilimnion, which attenuated these variations.

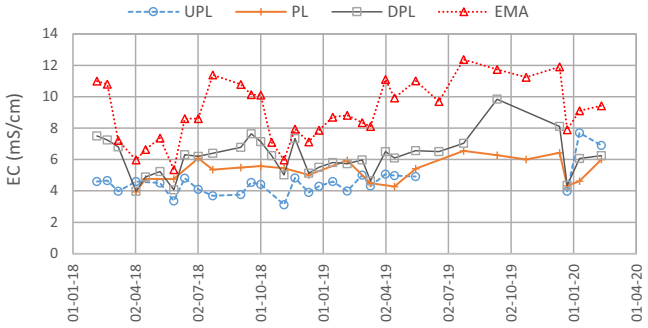

Fig. 3. Electrical conductivity (EC) evolution in the sampling points during the study period.

Table 2 shows the statistics of analytical results obtained during the different samplings. As can be seen, all samples contained high levels of dissolved sulfate, metals and metalloids (maximum values of 12.9 g/L of SO_4, 1.7 g/L of Fe, 724 mg/L of Al, 247 mg/L of Zn, 1.9 mg/L of As, etc.). Fig. 4 shows the concentrations for some representative elements as boxplot diagrams. For comparison purposes, the values obtained for the epilimnetic waters of the pit lake reported in previous works is also shown. As can be seen, values previously reported are in the same range than those found in this study, except for a very high Ca value reported in 2011 and a low value of Al in 2015. Therefore, these results confirm that the epilimnetic conditions in the pit lake have been approximately constant since 2006 (according to data from Sánchez España et al., 2008) despite its recent formation. In this sense, it has been previously reported a temporal hydrochemical evolution of pit lake waters until reaching a chemical equilibrium (e.g., Sánchez España et al., 2008; Moreno González et al., 2018; Juncosa et al., 2019).

In general, element concentration values are lower in UPL than in the rest of the points (Fig. 4). An increase is found in the pit lake (PL) with respect to UPL, while concentrations are approximately similar between PL and DPL. However, in the last point (EMA) a remarkable increase in concentrations can be seen (Fig. 4). Nevertheless, despite this general trend, some significant differences can be found between elements. Thus, the UPL point was characterized by showing the highest values for Mg and Ca (median of 403 mg/L and 166 mg/L, respectively), Al (121 mg/L) and Fe (119 mg/L).

Table 1
Statistics of physico-chemical parameters and flow rate during the study period.

	EC	pH	Eh	Q	NA	EC	pH	Eh	Q	NA
	mS/cm		mV	L/s	g/L $CaCO_3$	mS/cm		mV	L/s	g/L $CaCO_3$
	UPL					PL				
Mean	4.56	2.84	620	4.4	1.20	5.34	2.48	734	–	1.90
Median	4.52	2.80	645	2.3	1.09	5.43	2.57	773	–	1.76
25th perc.	3.98	2.70	625	0.6	0.85	4.74	2.45	755	–	1.67
75th perc.	4.83	3.00	680	6.5	1.38	6.00	2.65	791	–	2.01
Min.	3.12	2.20	201	0.0	0.60	3.95	1.36	206	–	1.56
Max.	7.70	3.47	718	16.3	2.57	6.55	2.81	854	–	3.53
	EC	pH	Eh	Q	NA	EC	pH	Eh	Q	NA
	mS/cm		mV	L/s	g/L $CaCO_3$	mS/cm		mV	L/s	g/L $CaCO_3$
	DPL					EMA				
Mean	6.21	2.43	675	13.4	2.12	9.07	2.36	612	14.2	4.87
Median	6.25	2.44	698	4.8	1.86	8.82	2.34	635	6.7	4.81
25th perc.	5.43	2.31	682	1.3	1.69	7.87	2.27	619	2.0	3.48
75th perc.	6.86	2.57	727	14.6	2.16	10.80	2.49	655	13.8	6.14
Min.	3.98	1.71	206	0.03	1.41	5.35	1.85	205	0.9	2.30
Max.	9.84	3.02	806	110.0	4.88	12.37	2.79	683	117.0	7.53

NA: Net acidity

Table 2
Statistics of analytical results obtained for the different sampling points.

	Al	Ca	Cu	Fe	K	Mg	Mn	Na	SO_4	Si	Zn	As	Cd	Cr	Li	Ni	Pb	Se	Sr	V	REE
	mg/L	mg/L	mg/L	mg/L	mg/L	mg/L	mg/L	mg/L	mg/L	mg/L	mg/L	µg/L	µg/L	µg/L	µg/L	µg/L	µg/L	µg/L	µg/L	µg/L	µg/L
UPL																					
Mean	137	171	13	138	2.6	444	34	18	3398	27	67	122	147	20	266	451	42	34	235	4.4	1383
Median	121	166	10	119	2.3	403	33	18	3233	26	63	24	133	9	226	397	35	33	208	2.6	1141
25th perc.	99	155	9	95	1.8	366	29	17	2665	23	52	16	99	6	152	294	23	20	187	1.6	1004
75th perc.	133	187	16	161	3.0	489	38	19	3648	28	72	100	176	17	364	563	40	40	301	8.0	1503
Min.	71	95	6	43	0.9	232	16	11	1802	15	28	5	83	3	124	194	18	12	119	1.0	702
Max.	370	300	30	357	8.3	930	70	22	6822	44	148	622	356	218	538	886	125	94	359	10	3439
PL																					
Mean	186	234	24	206	1.8	533	45	22	4523	36	89	97	203	20	327	463	66	45	283	2.9	1777
Median	178	230	23	212	1.6	534	44	22	4554	35	88	91	196	20	306	434	65	43	270	2.6	1780
25th perc.	171	220	22	195	1.4	484	42	20	4203	34	85	72	168	18	242	410	60	34	258	2.3	1650
75th perc.	186	242	24	218	2.0	568	47	23	4842	37	92	116	214	21	348	505	72	50	278	3.7	1833
Min.	165	206	21	147	0.1	438	39	17	3822	31	76	65	135	17	202	186	50	28	240	1.9	1455
Max.	284	273	28	230	3.7	647	52	33	5270	43	110	149	327	24	688	954	105	83	436	4.8	2460
DPL																					
Mean	213	241	28	285	1.5	515	44	21	4843	43	89	213	215	38	383	561	85	43	298	10	1819
Median	187	230	24	204	1.4	515	44	21	4655	37	87	91	191	29	327	521	72	43	273	4.1	1713
25th perc.	174	214	22	188	1.1	457	40	19	4333	33	81	49	171	23	280	429	57	33	258	3.2	1566
75th perc.	229	252	28	226	1.6	554	45	23	4997	49	89	119	232	42	512	662	112	52	292	6.6	1934
Min.	160	191	20	138	0.4	413	37	15	3828	29	74	13	137	8	210	98	16	26	228	1.7	1437
Max.	415	359	78	1223	2.5	772	63	25	8773	86	175	1925	389	119	674	963	186	65	515	70	2890
EMA																					
Mean	465	279	65	997	1.6	805	69	21	8926	54	168	200	420	111	846	1180	62	63	344	57	2367
Median	478	271	63	930	1.0	840	66	21	9115	50	173	103	420	92	820	1197	59	67	320	55	2250
25th perc.	356	244	48	670	0.7	647	58	20	6830	39	133	65	282	63	627	766	38	50	288	36	1994
75th perc.	579	306	80	1321	2.4	932	80	23	10,891	66	202	163	506	117	974	1421	75	73	362	76	2723
Min.	210	192	27	288	0.0	439	39	16	4842	30	94	18	179	27	281	467	7	27	231	7	1612
Max.	724	432	102	1680	4.5	1113	95	25	12,927	77	247	1518	812	514	1796	2315	195	95	685	105	3672

On the contrary, in EMA the highest concentration was found for Fe (median value of 930 mg/L) while contents of Al and Ca were much lower (median of 478 and 271 mg/L, respectively). Regarding As concentration, it shows an increase downstream, although with some outlier high values (Fig. 4). Moreover, the Pb concentrations in EMA are lower than those found in PL and DPL. Finally, concentrations of V were approximately constant in the three first sampling points while registered a sharp increase in EMA (Fig. 4).

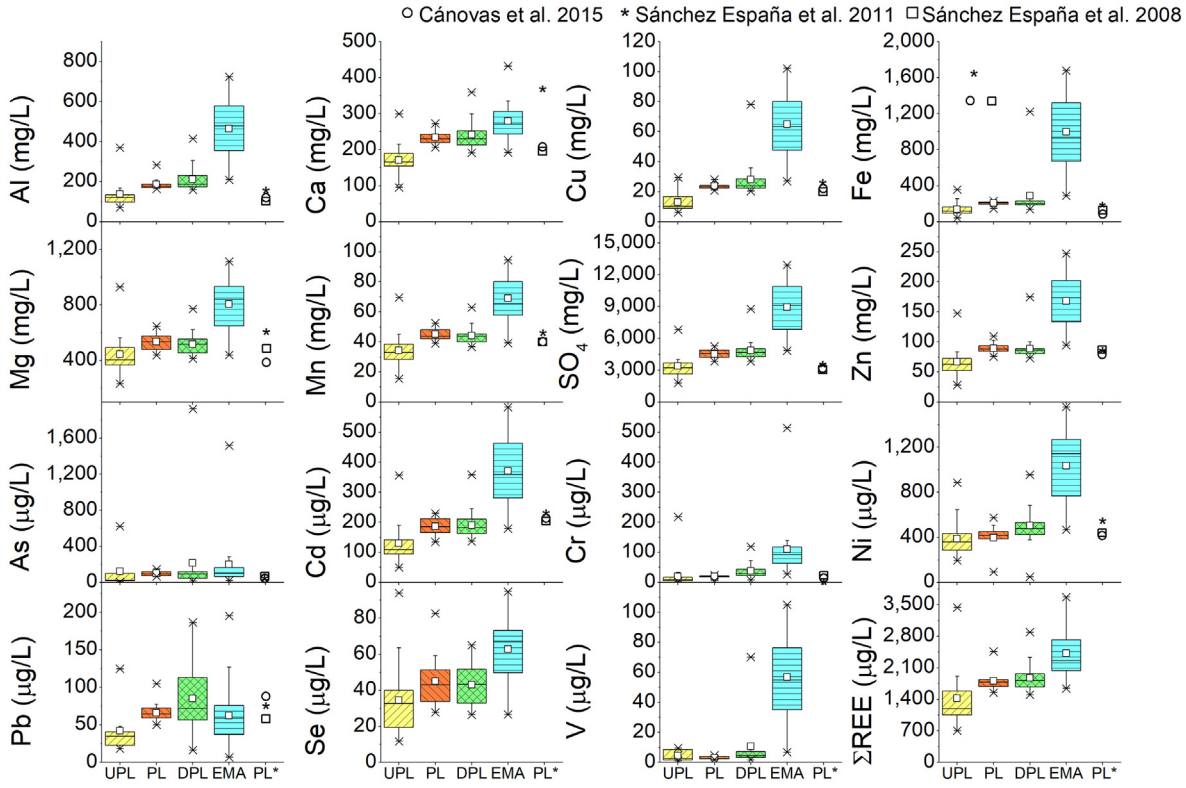

Fig. 4. Major and trace element concentrations represented as box plots diagrams from each sampling point. PL* shows data of the pit lake epilimnion from previous works.

Hydrochemical differences between sampling points can be more clearly observed in Fig. 5. Median concentrations for most elements (Al, Ca, Mg, Mn, Na, SO_4, Si, Zn, Cd, Ni, Se, Sr and REE) in the pit lake are between 1.2 and 1.5 higher than those found in UPL. Concentration by evaporation, especially during summer, might be the main reason of these differences, as it can be seen in both the EC tendency (Fig. 3) and element concentration (Fig. SM3) during this period. However, there must exist underground inputs into the pit lake, noticeably enriched with Cu, Fe, Pb, Cr and, especially, As, which cause a concentration increase to a greater extent with respect to UPL (e.g., up to 3.8 times higher for As; Fig. 5).

The similarity in element concentration between PL and DPL, with the exception of Cr and V concentration (Fig. 5), evidences the lack of significant pollutant discharges towards this zone from the W dumps. Thus, the hydrogeochemistry of DPL sampling point is chiefly controlled by the waters overflowing the pit lake. On the contrary, an important pollutant discharge from the W dumps is found between DPL and EMA sampling points. These discharges are especially enriched in V and, to a lesser extent, Al, Cu, Fe, SO_4, Zn, Cd, Cr and Ni (Fig. 5). On the other hand, the median concentration of Pb is lower in the final sampling point (EMA) than upstream (DPL and PL), as commented previously. The decrease in Pb concentration in sulfate-rich waters was previously observed in the IPB and other areas affected by AMD due to anglesite precipitation and/or coprecipitation of Pb with Fe-oxyhydroxysulfates (e.g., Acero et al., 2006; Nordstrom, 2011; Cánovas et al., 2016; Moreno González et al., 2020b).

Metal attenuation in mine sites by precipitation of secondary minerals constitutes a quantification of the importance of in-stream processes, which can be inferred by geochemical modeling (e.g., Runkel et al., 2012). In this sense, results from PHREEQC show oversaturation with respect to jarosite and schwermannite (Fig. 6), Fe minerals commonly precipitating in AMD environments. In general, saturation indices of these minerals are higher in the pit lake (PL) and lower in the EMA sampling point, although the highest levels of Fe and SO_4 are found in EMA (Fig. 4). This can be explained by the lower pH values in EMA, which counteracts the increase of concentrations observed in this point. Regarding soluble sulfate, the only mineral phase near saturation or slightly oversaturated in waters is gypsum, which experiences an increase in the saturation index along the water flow (Fig. 6). This explains the low increase of Ca concentration observed from UPL to EMA (Fig. 4), unlike other elements. Anglesite ($PbSO_4$) is undersaturated in all the samples, although with lower values observed in UPL, following the concentration pattern recorded (Fig. 4). On the other hand, copiapite and melanterite show values near saturation in the final point (EMA), where high amounts of efflorescence salts appear during dry periods (Fig. SM2).

4.3. NASC-normalized REE patterns

Rare earth elements have been traditionally used as geochemical tracer in aquatic systems (e.g., Worrall and Pearson, 2001; Wilkin et al., 2021). A statistical summary of REE concentrations in sampling points can be found in Table 2 while complete data can be consulted in Table SM1.

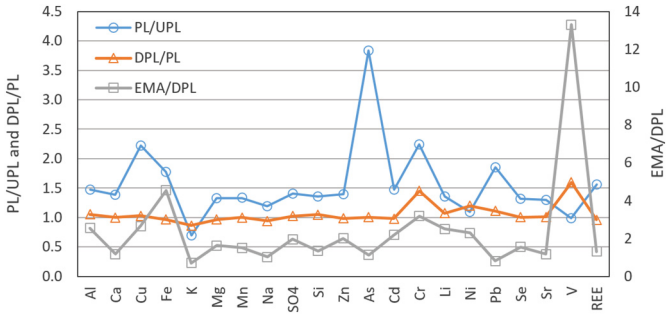

Fig. 5. Ratios of median concentrations between sampling points (EMA/DPL ratio is shown on a different scale because of its higher values).

Concentration of REE showed a similar tendency than most elements. Minimum concentrations were found in UPL (median value of 1.14 mg/L) while values in EMA were approximately twice (2.25 mg/L). These values are similar to those found in other mines from the IPB (Tharsis), being among the highest reported worldwide (Table 3).

Fig. 7 represents the REE NASC-normalized pattern for the different sampling points. Results show an enrichment in MREE in comparison to LREE and HREE, as previously reported in waters affected by AMD (Tabaksblat, 2002; Zhao et al., 2007; Soyol-Erdene et al., 2018). Negative anomalies of Eu can be also observed, with a mean value of 0.7. It is worth to notice the identical pattern in DPL and PL sampling points, which are also similar to that of UPL, although increased by a 1.5 factor due to evaporation from the pit lake. On the contrary, some differences can be observed in EMA with respect to DPL and PL, as LREE concentration experienced a lower increase than those recorded in MREE and HREE (e.g. the median value of La in EMA is 1.14 times higher than that of DPL, while for Lu it is 1.43). This indicates that inputs between DPL and EMA are mainly depleted in LREE, with respect other AMD sources in San Telmo.

4.4. Dissolved pollutant load

EMA sampling point collects all pollutants discharged by the different AMD sources in the study zone, which finally joins to the Oraque River, tributary of the Odiel River. Median values of pollutant load were 519 kg/day of Fe, 241 kg/day of Al and 88 kg/day of Zn, and so on, with peaks reaching even 2857 kg/day of Fe.

The main pollutants in the study area (between 50 and 70% of Al, Cd, Mg, Mn, Ni, SO_4 and Zn and more than 70% for Cu, Cr, Fe and, especially, V; Fig. 8) come from the west dumps located between DPL and EMA sampling points. On the other hand, AMD coming from the NE dumps is especially rich in Ca, Mg and REE, with more than 40% of the total load released from this area. Pollutant discharges from the pit lake, obtained as the difference between UPL and DPL, represent less than 15% for most elements, with the exception of As (54%) and Pb (64%). This information is crucial in order to develop and design restoration measurements in this mining area.

5. Conclusions

Water outputs from San Telmo pit lake are not permanent, but dependent on the balance between surface and groundwater inputs and the evaporation outputs. For example, rains in 2019 were scarce and thus, there were no surface water inputs to the pit lake. This fact, together with the high evaporation recorded caused the pit lake to behave as a terminal lake. However, during wetter periods, when rainfalls are abundant leading to increasing inputs, the pit lake behaves as flow-through type.

Concentrations in the epilimnetic pit lake waters were within the range found in previous studies. This implies that, despite its recent formation, hydrochemical conditions remain approximately constant for at least 15 years. The hydrochemistry of epilimnetic pit lake waters is mainly controlled by surface water inputs and the increase of element concentrations due to evaporation. REE NASC-normalized pattern are consistent with this result, highlighting the usefulness of REE as geochemical tracers in hydrological systems. In this sense, REE concentrations in this area are similar to those found in other mines from the IPB (Tharsis), being among the highest reported worldwide. Nevertheless, concentrations of As, Cr, Cu, Fe and Pb in the epilimnion experienced a higher increase than the rest of elements, with may be related to underground water inputs enriched in these elements.

Pollutant concentrations in the mining area increase notably downstream (from E to W), reaching maximum values of 1.7 g/L of Fe, 0.72 g/L of Al and 0.25 g/L of Zn at the outlet of the mining area. The main pollutant discharges are released between DPL and EMA sampling points, coming from the western waste dumps. These AMD discharges are especially enriched in V and, to a lesser extent, Fe and other elements. The pollutant

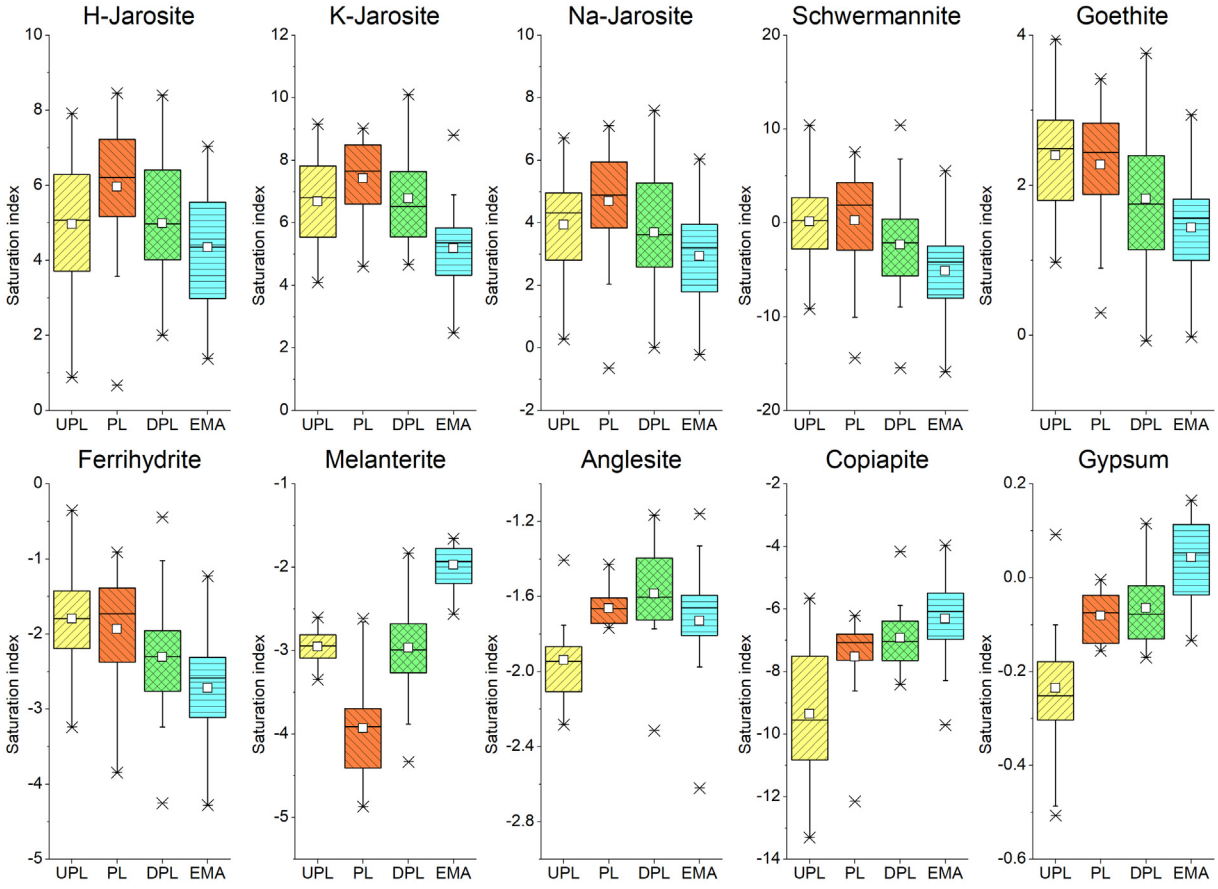

Fig. 6. Box plot diagrams of saturation indices of waters in sampling points with respect to some mineral phases commonly observed in AMD environments.

load delivered by the San Telmo mining area is very high, with median values of 519 kg/day of Fe, 241 kg/day of Al and 88 kg/day of Zn, deteriorating irreversibly the Oraque River, which will feed a reservoir currently under construction. These values are several orders of magnitude higher than those reported in other mine sites worldwide. Therefore, restoration measurements must be urgently performed in this area to reduce the impact caused in the water network downstream, especially in the water quality of the future reservoir. As pointed in this study, these actions must be prioritized in W dumps, due to its higher pollutant potential.

Table 3
Comparison of REE concentrations with other mining zones.

Site	pH	EC (mS/cm)	REE (μg/L)
San Telmo Upperstream Pit Lake (UPL)	2.8	4.5	1141
San Telmo Pit Lake (PL)	2.6	5.4	1780
San Telmo Downstream Pit Lake (DPL)	2.4	6.3	1713
San Telmo End Mining Area (EMA)	2.3	8.8	2250
Tharsis mine, IPB, Spain[a]	2.5	12.8	1747
Podwiśniówka acid pit lake, Poland[b]	2.4	–	993
Upper Rio Agrio, Patagonia, Argentina[c]	1.6	–	1637
Paradise Portal (PPREE1), CO, USA[d]	5.3	–	458
Ronneburg, Germany[e]	4.7	7.3	1387
Sitai coal mine, China[f]	3.6	–	61

[a] Moreno González et al. (2020b)
[b] Migaszewski et al. (2016)
[c] Gammons et al. (2005)
[d] Verplanck et al. (2001)
[e] Grawunder and Merten (2012)
[f] Zhao et al. (2007)

Supplementary data to this article can be found online at https://doi.org/10.1016/j.scitotenv.2022.155224.

CRediT authorship contribution statement

J.M Fuentes-López: Writing - Original Draft, Methodology, Writing - Review & Editing, **M. Olías:** Conceptualization, Funding acquisition, Investigation, Supervision, Writing - Review & Editing, **R. León:** Methodology; Writing - Review & Editing, **M.D Basallote:** Methodology; Writing - Review & Editing, **R. Moreno-González:** Methodology, Visualization, **F. Macías:** Formal Analysis, Validation, Writing - Review & Editing, **C.R Cánovas**: Conceptualization, Funding acquisition, Investigation, Supervision, Writing - Review & Editing.

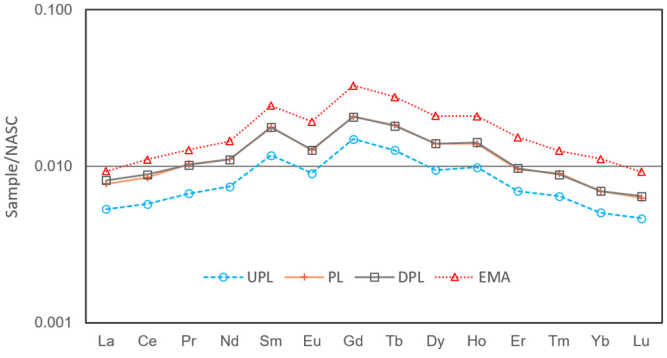

Fig. 7. REE NASC-normalized patterns for the median values of sampling points.

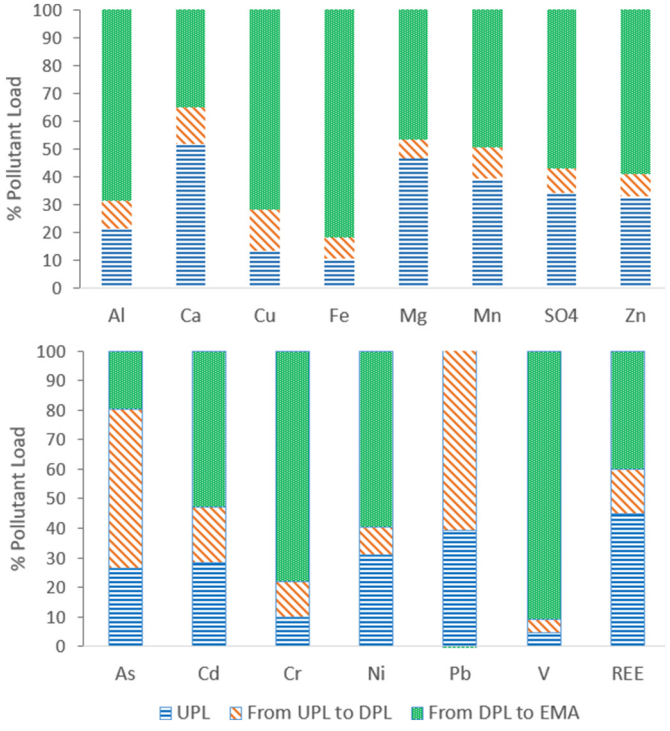

Fig. 8. Pollutant load contribution from the different mining components. UPL shows the pollutant load from the NE dumps entering the pit lake, 'From UPL to DPL' shows the contribution of the pit lake and 'From DPL to EMA' indicates the pollutant load increase observed between these sampling points delivered by the W waste dumps.

Declaration of competing interest

The authors declare that they have no known competing financial interests or personal relationships that could have appeared to influence the work reported in this paper.

Acknowledgements

This work was supported by the Spanish Ministry of Economic and Competitiveness through the projects CGL2016-78783-C2-1-R (SCYRE) and by H2020 European Institute of Innovation and Technology (EIT RawMaterials) through the projects Modular Recovery Process Services for Hydrometallurgy and Water Treatment (MORECOVERY). C.R Cánovas thanks the Spanish Ministry of Science and Innovation for the Postdoctoral Fellowship granted under application reference RYC2019-027949-I. F. Macias was funded by the R&D FEDER Andalucía 2014–2020 call through the project RENOVAME (FEDER; UHU-1255729). The comments and helpful criticisms of two anonymous reviewers and the support of Dr. Jose Virgilio Cruz (Associate Editor) have considerably improved the original manuscript and are also gratefully acknowledged. Funding for open access charge: Universidad de Huelva / CBUA

References

Acero, P., Ayora, C., Torrentó, C., Nieto, J.M., 2006. The behavior of trace elements during schwertmannite precipitation and subsequent transformation into goethite and jarosite. Geochim. Cosmochim. Acta 70 (16), 4130–4139. https://doi.org/10.1016/j.gca.2006.06.1367.

Almodóvar, G.R., Yesares, L., Sáez, R., Toscano, M., González, F., Pons, J.M., 2019. Massive sulfide ores in the Iberian Pyrite Belt: mineralogical and textural evolution. Minerals 9, 653. https://doi:10.3390/min9110653.

Blodau, C., 2006. A review of acidity generation and consumption in acidic coalmine lakes and their watersheds. Sci. Total Environ. 369, 307–332. https://doi.org/10.1016/j.citotenv.2006.05.004.

Cánovas, C.R., Peiffer, S., Macías, F., Olías, M., Nieto, J.M., 2015. Geochemical processes in a highly acidic pit lake of the Iberian Pyrite Belt (SW Spain). Chem. Geol. 395, 144–153. https://doi.org/10.1016/j.chemgeo.2014.12.007.

Cánovas, C.R., Macías, F., Pérez-López, R., 2016. Metal and acidity fluxes controlled by precipitation/dissolution cycles of sulfate salts in an anthropogenic mine aquifer. J. Contam. Hydrol. 188, 29–43. https://doi.org/10.1016/j.jconhyd.2016.02.005.

Castendyk, D.N., Eary, L.E., Balistrieri, L.S., 2015. Modeling and management of pit lake water chemistry 1: theory. Appl. Geochem. 57, 267–288. https://doi.org/10.1016/j.apgeochem.2014.09.004.

Diez Ercilla, M., López Pamo, E., Sánchez España, J., 2009. Photoreduction of Fe(III) in the acidic mine pit lake of San Telmo (Iberian Pyrite Belt): field and experimental work. Aquat. Geochem. 15 (3), 391–419. https://doi.org/10.1007/s10498-008-9044-1.

Donaire, T., Pascual, E., Sáez, R., Toscano, M., 2020. Facies architecture and palaeoenvironmental constraints of subaqueous felsic volcanism in the Iberian Pyrite Belt: the Paymogo volcano-sedimentary alignment. J. Volcanol. Geoth. Res. 405, 107045. https://doi.org/10.1016/j.jvolgeores.2020.107045.

Elghali, A., Benzaazoua, M., Bouzahzah, H., Abdelmoula, M., Dynes, J.J., Jamieson, H.E., 2021. Role of secondary minerals in the acid generating potential of weathered mine tailings: crystal-chemistry characterization and closed mine site management involvement. Sci. Total Environ. 784, 147105. https://doi.org/10.1016/J.SCITOTENV.2021.147105.

Erostate, M., Huneau, F., Garel, E., Vystavna, Y., Santoni, S., Pasqualini, V., 2019. Coupling isotope hydrology, geochemical tracers and emerging compounds to evaluate mixing processes and groundwater dependence of a highly anthropized coastal hydrosystem. J. Hydrol. 578, 123979. https://doi.org/10.1016/j.jhydrol.2019.123979.

Fan, R., Qian, G., Li, Y., Short, M.D., Schumann, R.C., Chen, M., Smart, R.S.C., Gerson, A.R., 2022. Evolution of pyrite oxidation from a 10-year kinetic leach study: implications for secondary mineralisation in acid mine drainage control. Chem. Geol. 588, 120653. https://doi.org/10.1016/j.chemgeo.2021.120653.

Galván, L., Olías, M., Cánovas, C.R., Sarmiento, A.M., Nieto, J.M., 2016. Hydrological modeling of a watershed affected by acid mine drainage (Odiel River, SW Spain). Assessment of the pollutant contributing areas. J. Hydrol. 540, 196–206. https://doi.org/10.1016/j.jhydrol.2016.06.005.

Gammons, C.H., Wood, S.A., Pedrozo, F., Varekamp, J.C., Nelson, B.J., Shope, C.L., Baffico, G., 2005. Hydrogeochemistry and rare earth element behavior in a volcanically acidified watershed in Patagonia, Argentina. Chem. Geol. 222 (3–4), 249–267. https://doi.org/10.1016/j.chemgeo.2005.06.002.

Grawunder, A., Merten, D., 2012. Rare earth elements in acidic systems – biotic and abiotic impacts. In: Kothe, E., Varma, A. (Eds.), Bio-geo Interactions in Metal-contaminated Soils. Soil Biology. 31. Springer, Berlin, Heidelberg. https://doi.org/10.1007/978-3-642-23327-2_4.

Johnson, D.B., Hallberg, K.B., 2005. Acid mine drainage remediation options: a review. Sci. Total Environ. 338, 3–14. https://doi.org/10.1016/j.scitotenv.2004.09.002.

Juncosa, R., Delgado, J., Cereijo, J.L., Muñoz, A., 2019. Hydrochemical evolution of the filling of the mining Lake of As Pontes (Spain). Mine Water Environ. 38 (3), 556–565. https://doi.org/10.1007/s10230-019-00612-6.

Kirby, C.S., Cravotta, C.A., 2005. Net alkalinity and net acidity 1: theoretical considerations. Appl. Geochem. 20 (10), 1920–1940. https://doi.org/10.1016/j.apgeochem.2005.07.002.

Luo, C., Routh, J., Dario, M., Sarkar, S., Wei, L., Luo, D., Liu, Y., 2020. Distribution and mobilization of heavy metals at an acid mine drainage affected region in South China, a post-remediation study. Sci. Total Environ. 724, 138122. https://doi.org/10.1016/j.scitotenv.2020.138122.

McCullough, C.D., 2015. Consequences and opportunities from river breach and decant of an acidic mine pit lake. Ecol. Eng. 85, 328–338. https://doi.org/10.1016/j.ecoleng.2015.10.001.

Migaszewski, Z.M., Galuszka, A., Gowska, S., 2016. Rare earth and trace element signatures for assessing an impact of rock mining and processing on the environment: wisniowka case study, south-central Poland. Environ. Sci. Pollut. Res. 23, 24943–24959. https://doi.org/10.1007/s11356-016-7713-y.

Moreno González, R., Olías, M., Macías, F., Cánovas, C.R., de Villarán, R.F., 2018. Hydrological characterization and prediction of flood levels of acidic pit lakes in the Tharsis mines, Iberian Pyrite Belt. J. Hydrol. 566, 807–817. https://doi.org/10.1016/j.jhydrol.2018.09.046.

Moreno González, R., Cánovas, C.R., Olías, M., Macías, F., 2020a. Seasonal variability of extremely metal rich acid mine drainages from the Tharsis mines (SW Spain). Environ. Poll. 259, 113829. https://doi.org/10.1016/j.envpol.2019.113829.

Moreno González, R., Cánovas, C.R., Olías, M., Macías, F., 2020b. Rare earth elements in a historical mining district (south-west Spain): hydrogeochemical behaviour and seasonal variability. Chemosphere 253, 1–10. https://doi.org/10.1016/j.chemosphere.2020.126742.

Newman, C.P., Poulson, S.R., McCrea, K.M., 2020. Contaminant generation and transport from mine pit lake to perennial stream system: multidisciplinary investigations at the Big Ledge Mine, Nevada, USA. Geochemistry https://doi.org/10.1016/j.chemer.2019.125552.

Nordstrom, D.K., 2011. Hydrogeochemical processes governing the origin, transport and fate of major and trace elements from mine wastes and mineralized rock to surface waters. Appl. Geochem. 26 (11), 1777–1791. https://doi.org/10.1016/j.apgeochem.2011.06.002.

Nordstrom, D.K., Wilde, F.D., 1998. Reduction-Oxidation Potential (Electrode Method). 9. U.S. Geological Survey TQRI Book, pp. 1–20.

Olías, M., Nieto, J.M., Sarmiento, A.M., Cánovas, C.R., Galván, L., 2011. Water quality in the future Alcolea Reservoir (Odiel River, SW Spain): a clear example of the inappropriate management of water resources in Spain. Water Resour. Manag. 25, 201–215. https://doi.org/10.1007/s11269-010-9695-8.

Olías, M., Cánovas, C.R., Basallote, M.D., Macías, F., Pérez-López, R., González, R.M., Millán-Becerro, R., Nieto, J.M., 2019. Causes and impacts of a mine water spill from an acidic pit lake (Iberian Pyrite Belt). Environ. Poll. 250, 127–136. https://doi.org/10.1016/j.envpol.2019.04.011.

Olías, M., Cánovas, C.R., Macías, F., Basallote, M.D., Nieto, J.M., 2020. The evolution of pollutant concentrations in a river severely affected by acid mine drainage: Río tinto (SW Spain). Minerals 10 (7). https://doi.org/10.3390/min10070598.

Parkhurst, D.L., Appelo, C.A.J., 2013. Description of Input and Examples for PHREEQC Version 3 — A Computer Program for Speciation, Batch-reaction, One-dimensional Transport, and Inverse Geochemical Calculations. U.S. Geological Survey Techniques and Methods, Book 6, Chapter A43, 497 p. U.S. Geological Survey Techniques and Methods, Book 6, Chapter A43, 6-43A.

Pellicori, D.A., Gammons, C.H., Poulson, S.R., 2005. Geochemistry and stable isotope composition of the Berkeley pit lake and surrounding mine waters, Butte, Montana. Appl. Geochem. 20 (11), 2116–2137. https://doi.org/10.1016/j.apgeochem.2005.07.010.

Pinedo Vara, I., 1963. Piritas de Huelva. Su historia, minería y aprovechamiento. Summa, Madrid.

Rinder, T., Dietzel, M., Stammeier, J.A., Leis, A., Bedoya-González, D., Hilberg, S., 2020. Geochemistry of coal mine drainage, groundwater, and brines from the Ibbenbüren mine, Germany: a coupled elemental-isotopic approach. Appl. Geochem. 121, 104693. https://doi.org/10.1016/j.apgeochem.2020.104693.

Ríos, C.A., Williams, C.D., Roberts, C.L., 2008. Removal of heavy metals from acid mine drainage (AMD) using coal fly ash, natural clinker and synthetic zeolites. J. Hazard. Mater. 156 (1–3), 23–35. https://doi.org/10.1016/j.jhazmat.2007.11.123.

Runkel, R.L., Kimball, B.A., Walton-Day, K., Verplanck, P.L., Broshears, R., 2012. Evaluating remedial alternatives for an acid mine drainage stream: a model post audit. Environ. Sci. Technol. 46, 340–347. https://doi.org/10.1021/es2038504.

Sánchez España, J., Pamo, E.L., Santofimia, E., Aduvire, O., Reyes, J., Barettino, D., 2005. Acid mine drainage in the Iberian Pyrite Belt (Odiel river watershed, Huelva, SW Spain): geochemistry, mineralogy and environmental implications. Appl. Geochem. 20 (7), 1320–1356. https://doi.org/10.1016/j.apgeochem.2005.01.011.

Sánchez España, J., Santofimia Pastor, E., González Toril, E., San Martín-Uriz, P., López Pamo, E., Amils, R., 2007. Physicochemical and microbiological stratification of a meromictic, acidic mine pit lake (San Telmo, Iberian Pyrite Belt). Proceedings of the IMWA Symposium Water in Mining Environment, pp. 446–451.

Sánchez España, J., Pamo, E.L., Pastor, E.S., Ercilla, M.D., 2008. The acidic mine pit lakes of the Iberian Pyrite Belt: an approach to their physical limnology and hydrogeochemistry. Appl. Geochem. 23 (5), 1260–1287. https://doi.org/10.1016/j.apgeochem.2007.12.036.

Sánchez España, J., Pamo, E.L., Diez, M., Santofimia, E., 2009. Physico-chemical gradients and meromictic stratification in Cueva de la Mora and other acidic pit lakes of the Iberian Pyrite Belt. Mine Water Environ. 28 (1), 15–29. https://doi.org/10.1007/s10230-008-0059-z.

Sánchez-España, J., Yusta, I., Diez-Ercilla, M., 2011. Schwertmannite and hydrobasaluminite: a re-evaluation of their solubility and control on the iron and aluminium concentration in acidic pit lakes. Appl. Geochem. 26 (9–10), 1752–1774. https://doi.org/10.1016/j.apgeochem.2011.06.020.

Sarmiento, A.M., Nieto, J.M., Olías, M., Cánovas, C.R., 2009. Hydrochemical characteristics and seasonal influence on the pollution by acid mine drainage in the Odiel river basin (SW Spain). Appl. Geochem. 24 (4), 697–714. https://doi.org/10.1016/j.apgeochem.2008.12.025.

Schafer, W.M., Croall, J., Schmidt, J., 2020. Predicting water quality trends in Lone Tree pit lake, Nevada (USA). Mine Water Environ. 39, 618–629. https://doi.org/10.1007/s10230-020-00698-3.

Soyol-Erdene, T.O., Valente, T., Grande, J.A., de la Torre, M.L., 2018. Mineralogical controls on mobility of rare earth elements in acid mine drainage environments. Chemosphere 205, 317–327. https://doi.org/10.1016/j.chemosphere.2018.04.095.

Tabaksblat, L.S., 2002. Specific features in the formation of the mine water microelement composition during ore mining. Water Resour. 29 (3), 333–345. https://doi.org/10.1023/A:1015640615824.

Taylor, S.R., McLennan, S.M., 1985. The Continental Crust: Its Composition and Evolution. Blackwell Scientific Publications, Oxford.

Tomiyama, S., Igarashi, T., Tabelin, C.B., Tangviroon, P., Ii, H., 2019. Acid mine drainage sources and hydrogeochemistry at the Yatani mine, Yamagata, Japan: a geochemical and isotopic study. J. Contam. Hydrol. 225, 103502. https://doi.org/10.1016/j.jconhyd.2019.103502.

Torres, E., Ayora, C., Cánovas, C.R., García-Robledo, E., Galván, L., Sarmiento, A.M., 2013. Metal cycling during sediment early diagenesis in a water reservoir affected by acid mine drainage. Sci. Total Environ. 461–462, 416–429. https://doi.org/10.1016/j.scitotenv.2013.05.014.

Triantafyllidis, S., Skarpelis, N., 2006. Mineral formation in an acid pit lake from a high-sulfidation ore deposit: Kirki, NE Greece. J. Geochem. Explor. 88 (1-3), 68–71. https://doi.org/10.1016/j.gexplo.2005.08.017.

Valente, T., Grande, J.A., de la Torre, M.L., Santisteban, M., Cerón, J.C., 2013. Mineralogy and environmental relevance of AMD-precipitates from the Tharsis mines, Iberian Pyrite Belt (SW, Spain). Appl. Geochem. 39, 11–25. https://doi.org/10.1016/j.apgeochem.2013.09.014.

Verplanck, P.L., Antweiler, R.C., Nordstrom, D.K., Taylor, H.E., 2001. Standard reference water samples for rare earth element determinations. Appl. Geochem. 16 (2), 231–244. https://doi.org/10.1016/S0883-2927(00)00030-5.

Wendt-Potthoff, K., Koschorreck, M., Diez Ercilla, M., Sánchez España, J., 2012. Microbial activity and biogeochemical cycling in a nutrient-rich meromictic acid pit lake. Limnologica 42 (3), 175–188. https://doi.org/10.1016/j.limno.2011.10.004.

Wilkin, R.T., Lee, T.R., Ludwig, R.D., Wadler, C., Brandon, W., Mueller, B., Davis, E., Luce, D., Edwards, T., 2021. Rare-earth elements as natural tracers for in situ remediation of groundwater. Environ. Sci. Technol. 55 (2), 1251–1259. https://doi.org/10.1021/acs.est.0c06113.

Worrall, F., Pearson, D.G., 2001. Water-rock interaction in an acidic mine discharge as indicated by rare earth element patterns. Geochim. Cosmochim. Acta 65 (18), 3027–3040. https://doi.org/10.1016/S0016-7037(01)00662-7.

Yang, N., Zhou, P., Wang, G., Zhang, B., Shi, Z., Liao, F., Li, B., Chen, X., Guo, L., Dang, X., Gu, X., 2021. Hydrochemical and isotopic interpretation of interactions between surface water and groundwater in Delingha, Northwest China. J. Hydrol. 598, 126243. https://doi.org/10.1016/j.jhydrol.2021.126243.

Yu, J.Y., Heo, B., Choi, I.K., Cho, J.P., Chang, H.W., 1999. Apparent solubilities of schwertmannite and ferrihydrite in natural stream waters polluted by mine drainage. Geochim. Cosmochim. Acta 63 (19–20), 3407–3416. https://doi.org/10.1016/S0016-7037(99)00261-6.

Zhao, F., Cong, Z., Sun, H., Ren, D., 2007. The geochemistry of rare earth elements (REE) in acid mine drainage from the Sitai coal mine, Shanxi Province, North China. Int. J Coal Geol. 70 (1-3), 184–192. https://doi.org/10.1016/j.coal.2006.01.009.

Zhao, H., Xia, B., Qin, J., Zhang, J., 2012. Hydrogeochemical and mineralogical characteristics related to heavy metal attenuation in a stream polluted by acid mine drainage: a case study in Dabaoshan Mine, China. J. Environ. Sci. China 24 (6), 979–989. https://doi.org/10.1016/S1001-0742(11)60868-1.